

Complex Dynamic Behavior During Transition in a Solid Combustion Model

Through examples in a free-boundary model of solid combustion, this study concerns nonlinear transition behavior of small disturbances of front propagation and temperature as they evolve in time. This includes complex dynamics of period doubling, and quadrupling, and it eventually leads to chaotic oscillations. Within this complex dynamic domain we also observe a period six-folding. Both asymptotic and numerical solutions are studied. We show that for special parameters our asymptotic method with some dominant modes captures the formation of coherent structures. Finally, we discuss possible methods to improve our prediction of the solutions in the chaotic case. © 2009 Wiley Periodicals, Inc. Complexity 14: 9–14, 2009

1. INTRODUCTION

We study the nonuniform dynamics of front propagation in solid combustion: a chemical reaction that converts a solid fuel directly into solid products with no intermediate gas phase formation. For example, in self-propagating high-temperature synthesis (SHS), a flame wave advancing through powdered ingredients leaves high-quality ceramic materials or metallic alloys in its wake (see, for instance, [1]).

The propagation results from the interplay between heat generation and heat diffusion in the medium. A balance exists between the two in some parametric regimes, producing a constant burning rate. In other cases, competition between reaction and diffusion results in a wide variety of nonuniform behaviors, some leading to chaos.

In studying the nonlinear transition behavior of small disturbances of front propagation and temperature as they evolve in time, we compare quantitatively the results of weakly nonlinear analysis with direct simulations. We also propose techniques for the accurate simulation of chaotic solutions.

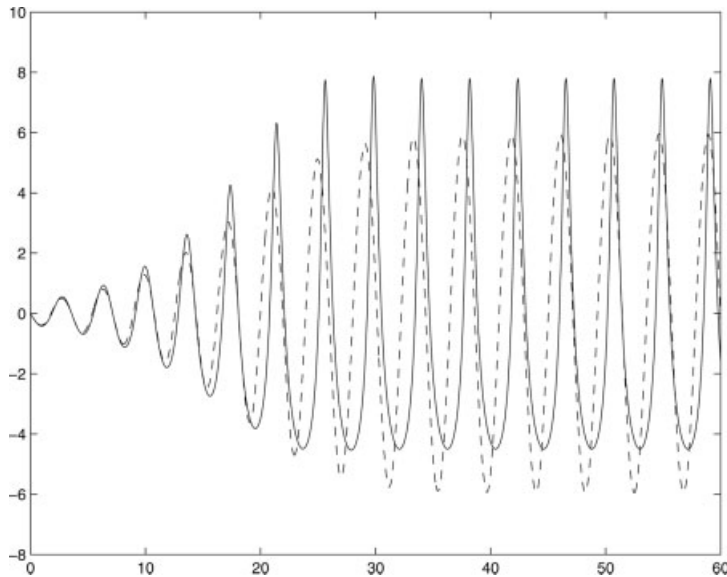
**JUN YU, LAURA K. GROSS, AND
CHRISTOPHER M. DANFORTH**

Jun Yu and Christopher M. Danforth are with the University of Vermont, Burlington, Vermont 05401. (e-mail: jun.yu@uvm.edu)

Laura K. Gross is with the University of Akron, Akron, Ohio 44325

This article was submitted as an invited paper at the Understanding Complex Systems conference held at the University of Illinois at Urbana, Champaign, May 2007.

FIGURE 1



Velocity perturbation versus time: comparison between numerical (solid line) and asymptotic (dashed line) for Arrhenius kinetics, $\sigma = 0.48$, $\epsilon = 0.1$, $A(0) = 0.1$ ($\nu \approx \nu_c - \epsilon^2 = 1/3 - (0.1)^2 = 0.323$).

2. MATHEMATICAL ANALYSIS

We use a version of the sharp-interface model of solid combustion introduced by Matkowsky and Sivashinsky [2]. It includes the heat equation on a semi-infinite domain and a nonlinear kinetic condition imposed on the moving boundary.

Specifically, we seek the temperature distribution $u(x, t)$ in one spatial dimension and the interface position $\Gamma(t) = \{x| x = f(t)\}$ that satisfy the appropriately nondimensionalized free-boundary problem

$$\frac{\partial u}{\partial t} = \frac{\partial^2 u}{\partial x^2}, \quad x > f(t), \quad t > 0, \quad (1)$$

$$V = G(u|_{\Gamma}), \quad t > 0, \quad (2)$$

$$\frac{\partial u}{\partial x} \Big|_{\Gamma} = -V, \quad t > 0. \quad (3)$$

Here V is the velocity of the rightward-traveling interface, i.e. $V = df/dt$. In addition, the temperature satisfies the condition $u \rightarrow 0$ as $x \rightarrow \infty$; that is,

the ambient temperature is normalized to zero at infinity.

To model solid combustion, we take the Arrhenius function as the kinetics function G in the nonequilibrium interface condition (2) [3, 4]. Then, with appropriate nondimensionalization, the velocity of propagation relates to the interface temperature as

$$V = \exp \left[\left(\frac{1}{\nu} \right) \frac{u - 1}{\sigma + (1 - \sigma)u} \right] \quad (4)$$

at the interface Γ . Here ν is inversely proportional to the activation energy of the exothermic chemical reaction that occurs at the interface, and $0 < \sigma < 1$ is the ambient temperature nondimensionalized by the adiabatic temperature of combustion products [5].

It is convenient to study the free-boundary problem in the following front-attached coordinate frame:

$$\eta = x - f(t), \quad \tau = t, \quad (5)$$

as the boundary conditions are now evaluated at $\eta = 0$ [6].

The free-boundary problem admits a traveling-wave solution.

$$u(\eta, \tau) = \exp(-\eta), \quad f(\tau) = \tau, \quad (6)$$

which is linearly unstable when ν is less than the critical value $\nu_c = 1/3$ (see, for example, [7, 8]). The discrete spectrum values are zero and

$$\lambda = \frac{1 - 3\nu \pm \sqrt{(3\nu - 1)^2 - 4\nu^3}}{2\nu^2}. \quad (7)$$

The eigenfunction corresponding to the eigenvalue λ is

$$g(\eta; \lambda, \nu) = (1 + \nu\lambda) \times \exp \left(-(1 + \sqrt{1 + 4\lambda}) \frac{\eta}{2} \right) - \exp(-\eta). \quad (8)$$

2.1. Asymptotic Solution

For the weakly nonlinear analysis, let ϵ^2 be a small deviation from the neutrally stable value of ν , namely

$$\epsilon^2 = \nu_c - \nu = \frac{1}{3} - \nu. \quad (9)$$

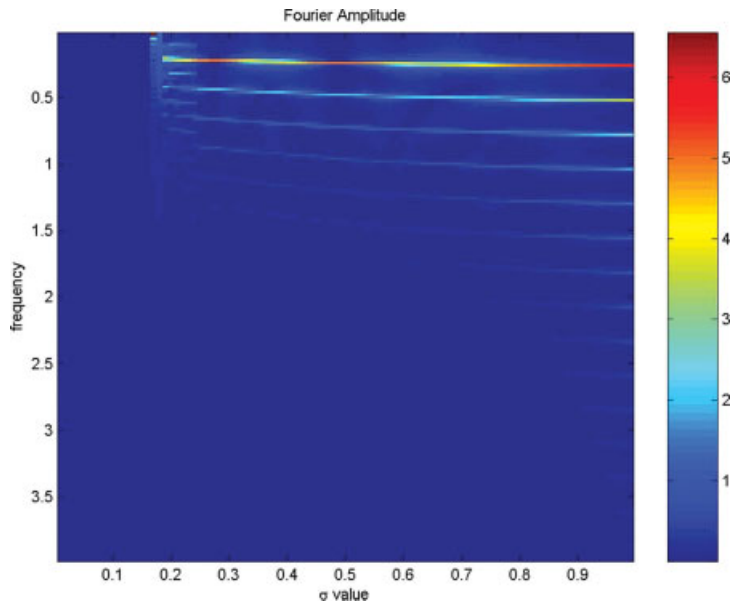
We refer this as marginally unstable case. We perturb the basic solution (6) by ϵ times the most linearly unstable mode given by (8), evaluated at both the neutrally stable parameter value $\nu = 1/3$ and the corresponding neutrally stable eigenvalue from (7), i.e.,

$$u(\eta, t_0, t_1, t_2) = e^{-\eta} + \epsilon A(t_1, t_2) e^{i\sqrt{3}t_0} g \left(\eta; i\sqrt{3}, \frac{1}{3} \right) + \epsilon^2 w_2(\eta, t_0, t_1, t_2) + \dots + \text{CC}, \quad (10)$$

where $t_0 = \tau$, and $t_1 = \epsilon\tau$ and $t_2 = \epsilon^2\tau$ are slow times, $A(t_1, t_2)$ is complex, and “CC” stands for complex-conjugate terms [6]. In the velocity expansion, we have

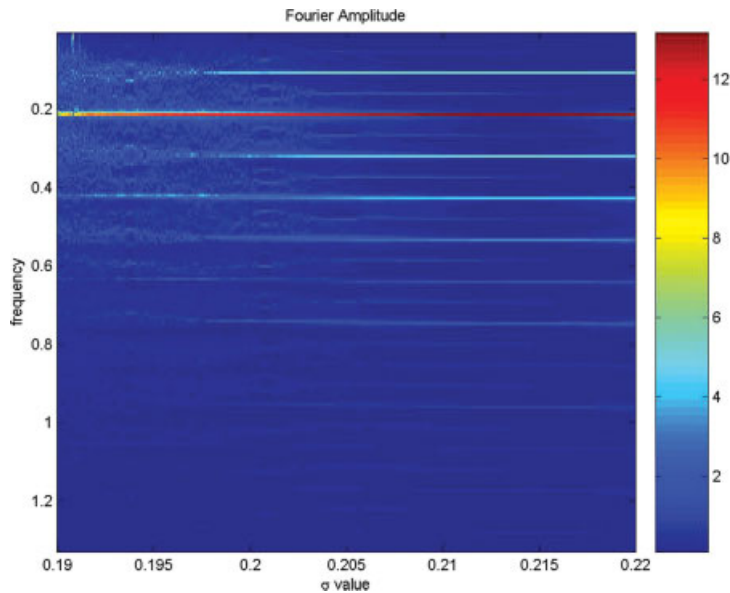
$$f(t_0, t_1, t_2) = t_0 + \epsilon \left[A(t_1, t_2) e^{i\sqrt{3}t_0} + \frac{1}{2} B(t_1, t_2) \right] + \epsilon^2 \phi_2(t_0, t_1, t_2) + \dots + \text{CC}, \quad (11)$$

FIGURE 2



Amplitudes corresponding to each frequency of the Fourier transformed velocity perturbation data for the Arrhenius kinetics parameter σ in the interval $(0, 1)$, $\epsilon = 0.1$, $A(0) = 0.1$, $35 < t < 85$ ($\nu \approx \nu_c - \epsilon^2 = 1/3 - (0.1)^2 = 0.32\bar{3}$).

FIGURE 3



Amplitudes corresponding to each frequency of the Fourier transformed velocity perturbation data for the Arrhenius kinetics parameter σ in the interval $(0.19, 0.22)$, $\epsilon = 0.1$, $A(0) = 0.1$, $35 < t < 85$ ($\nu \approx \nu_c - \epsilon^2 = 1/3 - (0.1)^2 = 0.32\bar{3}$).

where the real function $B(t_1, t_2)$ modulates the constant-velocity solution to the linearized problem.

As given in (10) the normal-mode perturbation is modulated by a complex-valued, slowly varying amplitude function $A(t_1, t_2)$. It turns out that the amplitude envelope does not explicitly depend on t_1 and as a function of t_2 it satisfies the solvability condition

$$\frac{dA}{dt_2} = \chi A + \beta A^2 \bar{A}, \quad (12)$$

where χ and β are complex constants (see [6] for details). Similarly,

$$\frac{dB}{dt_1} = r_0 A \bar{A}, \quad (13)$$

where r_0 is a real constant.

The evolution Eq. (12) has circular limit cycles in the complex- A plane for all values of the kinetic parameter σ in the interval $0 < \sigma < 1$ (i.e. for all physical values of σ). To find $A(t_2)$, we integrate the ordinary differential Eq. (12) using a fourth-order Runge–Kutta method. Once we obtain the value for $A(t_2)$, the asymptotic solution is available from (10), (8), (13), and (11).

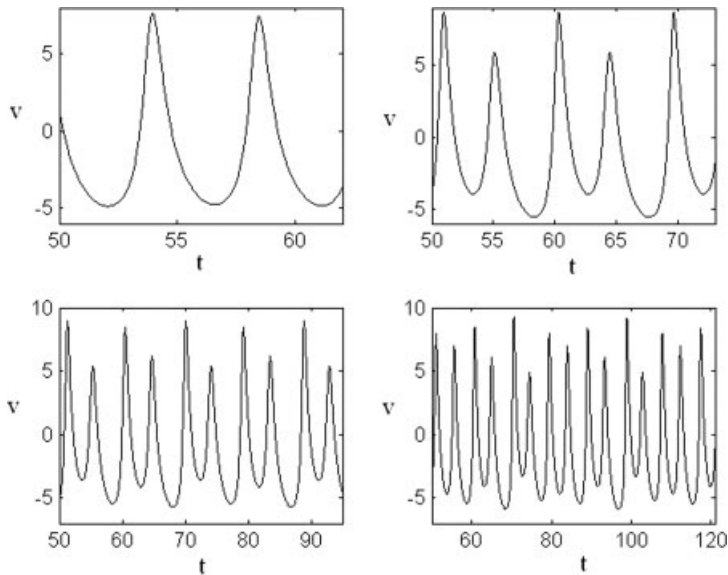
3. RESULTS AND DISCUSSION

To compare quantitatively the asymptotics with numerics, we first consider $\epsilon = 0.1$. The value of ν remains at the marginally unstable value $\nu_c - \epsilon^2$, as in Eq. (9), so $\nu \approx 0.32\bar{3}$. We show in this section that this choice of ϵ corresponds to a mix of dynamics as σ varies. Subsequently, we comment on the impact on the front behavior of both decreasing and increasing ϵ .

To start, take $\sigma = 0.48$ in the kinetics function (4). To observe the growth behavior of the solution, we take the initial condition $A(0) = 0.1$ for the remainder of this paper, unless otherwise indicated.

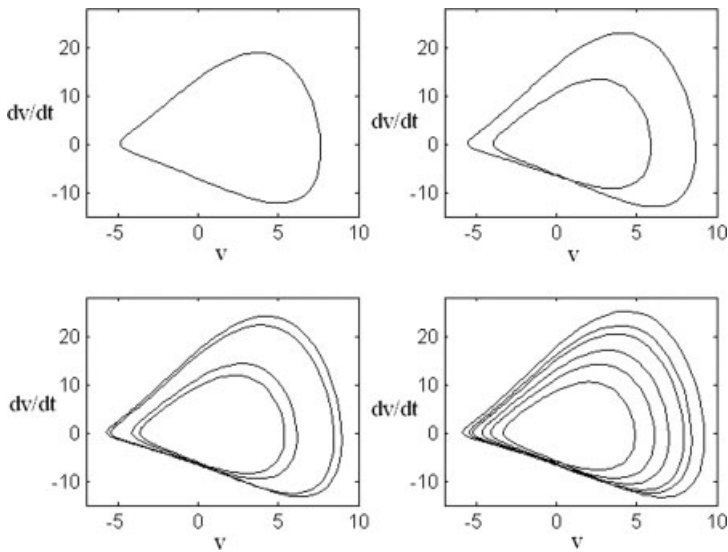
Figure 1 shows the numerical (solid line) and asymptotic (dashed line) values of front velocity perturbation as a function of time t in the interval $0 \leq t \leq 60$. To find the numerical solution, we used

FIGURE 4



Velocity perturbations versus time ($\epsilon = 0.1, A(0) = 0.1, v \approx v_c - \epsilon^2 = 1/3 - (0.1)^2 = 0.32\bar{3}$) clockwise from upper left: periodic solution for $\sigma = 0.48$ (cf. Figure 1), period doubling ($\sigma = 0.22$), period quadrupling ($\sigma = 0.21$), period six-folding ($\sigma = 0.20075$).

FIGURE 5



Phase plots of the four solutions in Figure 4: velocity perturbation $v(t)$ versus dv/dt .

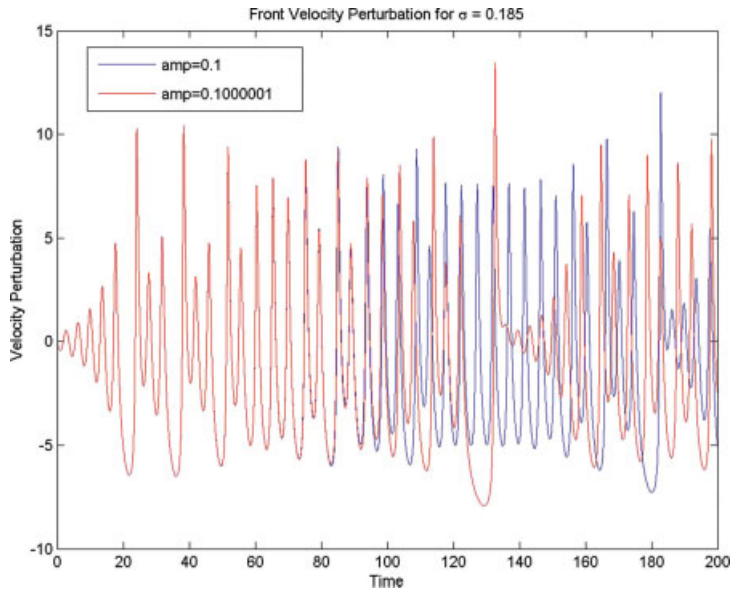
the Crank–Nicholson method to solve the problem in a front-attached coordinate frame, reformulating the boundary condition (3) for robustness (see [6] for details). As for the asymptotic solution, the previous section describes the order- ϵ perturbation to the traveling-wave solution (6).

Figure 1 reveals that from $t = 0$ to approximately $t = 30$, the small front velocity perturbation is linearly unstable, and its amplitude grows exponentially in time. As this amplitude becomes large, nonlinearity takes effect. At around $t = 30$, the front velocity perturbation has reached steady oscillation. The asymptotic solution accurately captures the period in both transient behavior for $t = 0$ to 30 and the long-time behavior after $t = 30$. The amplitude and phase differ somewhat. This is an example in which the weakly nonlinear approach describes well the marginally unstable large-time behaviors: A single modulated temporal mode captures the dynamics.

To identify additional such regimes systematically, we calculate numerically the velocity perturbation data on the time interval $35 < t < 85$, throughout the range of physical values of the kinetics parameter σ (i.e. $0 < \sigma < 1$, with $\Delta\sigma = 0.01$). Figure 2 summarizes the Fourier transformed velocity data. For each σ value and each frequency, the color indicates the corresponding amplitude, with the red end of the spectrum standing for larger numbers than the violet end. For roughly $0.3 < \sigma < 0.6$, the figure shows the dominance of the lowest-order mode, suggesting the appropriateness of the weakly nonlinear analysis in this range. For other values of σ , a single mode cannot be expected to capture the full dynamics of the solution.

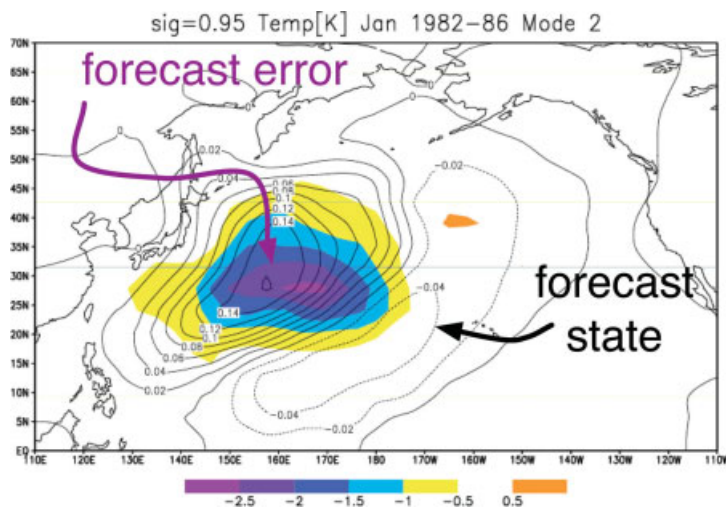
In particular, when σ is greater than approximately 0.6, solutions have sharp peaks, even sharper than the numerical solution in Figure 1. Figure 2 shows that when σ is smaller than approximately 0.3, the Fourier spectrum has a complicated character, starting with the emergence of a period-doubling solution for $\sigma \approx 0.25$. Figure 3

FIGURE 6



Velocity perturbation versus time: numerical solution for $\sigma = 0.185$, $\epsilon = 0.1$, $A(0) = 0.1$, and $A(0) = 0.1000001$ ($v \approx v_c - \epsilon^2 = 1/3 - (0.1)^2 = 0.32\bar{3}$).

FIGURE 7



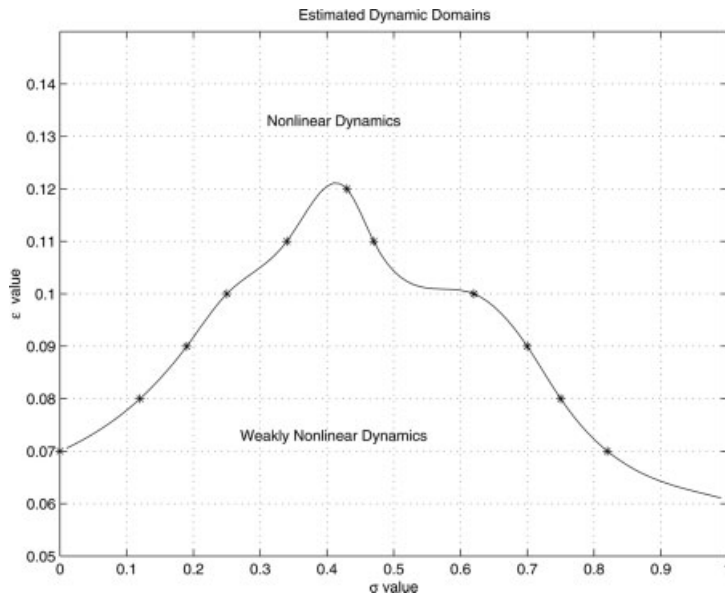
Curves of predicted (constant) near sea-surface temperature, along with colored bands of associated error (courtesy of [10]).

gives a closer look at the dominant modes for the case of small σ (with $\Delta\sigma = 0.00005$); period-quadrupling occurs for $\sigma \approx 0.0213$. Notice the bifurcation to a six-folding solution for $\sigma \approx 0.201$. In the first three panels in Figures 4 and 5 we demonstrate the cascade of period-replicating solutions, including doubling ($\sigma = 0.22$) and quadrupling ($\sigma = 0.21$). The number four panel in Figures 4 and 5 illustrates a six-folding solution at $\sigma = 0.20075$. Note that Figure 2 reflects the non-periodic solution for σ less than approximately 0.15.

The cascade of period-replicating solutions for decreasing σ leads to chaos. Figure 6 (corresponding to $\sigma = 0.185$) shows the sensitivity of the velocity perturbation to initial conditions. In the figure, note that from $t = 0$ to approximately $t = 25$, the small front speed perturbation is linearly unstable, and its amplitude grows exponentially in time, similar to the profile in Figure 1. As the amplitude becomes large, nonlinearity again comes into play. Still, the curves corresponding to two initial conditions (one with $A(0) = 0.1$ and the other with $A(0) = 0.1000001$) remain indistinguishable for a long time. However, as time approaches 100 the two profiles begin to diverge, and as time evolves past 120 they disagree wildly.

We propose a couple of techniques to improve model predictions in the chaotic case. One ensemble forecasting requires the generation of velocity profiles that correspond to slightly different initial conditions. The degree of agreement among curves in the collection (ensemble) demonstrates the level of reliability of predictions. In the spirit of the jet-stream forecasts in [9], additional data can be provided at the points at which the individual members of the ensemble diverge. For example, Figure 6, which shows an “ensemble” of only two curves, gives a preliminary indication of the need for more data at $t = 100$.

Alternatively, we can more accurately represent solid combustion by using statistical methods to “train” the model. Comparisons with experimental data

FIGURE 8

σ -Interval as a function of ϵ , which shows the domain of applicability of the weakly nonlinear analysis.

can reveal systematic and predictable error, as in Figure 7 (courtesy of [10]). The figure, which provides an analogy to the problem under consideration, shows that temperature forecasts made by a weather model for the sea surface off the coast of Japan are typically too warm [10]. That is, the actual temperatures minus the predicted temperatures

are negative values, represented as yellow, blue, and violet in the figure. In describing combustion, as in describing sea temperatures, one can compensate systematically for such error.

As the bifurcation parameter ν approaches ever closer to the neutrally stable value (i.e. as ϵ decreases), the complex dynamics—including chaos—

disappear. For example, when $\epsilon = 0.06$, the asymptotic and numerical solutions agree closely throughout the physical range of σ ($0 < \sigma < 1$). By contrast, when ϵ grows to 0.12, the σ interval in which one mode dominates strongly has a length of only 0.01. Figure 8 shows the σ -interval as a function of ϵ (with the values of the line obtained by polynomial interpolation). Varying ϵ quantifies the domain of applicability of the weakly nonlinear analysis and delineates the role of σ in the dynamics [6].

In summary, linear instability provides a mechanism for transition to nonlinear coherent structures. Weakly nonlinear analysis allows the asymptotic study of the evolution of small disturbances during this transition, providing insight into nonlinear dynamics, which can be investigated numerically.

The period six-folding solution found at $\sigma \approx 0.201$ is probably a coherent pattern within the chaotic domain. As σ values changing from 0.213 to ~ 0.202 the solution may have already gone through period-replicating and become chaotic, and these bifurcation details may require higher accuracy model to observe.

We also proposed techniques to improve predictions of solution behavior in the chaotic case. The ensemble method may provide accuracy over long time intervals. Also, given experimental data, statistical procedures can be used to train the model.

REFERENCES

1. Merzhanov, A.G. SHS processes: Combustion theory and practice. *Arch Combust* 1981, 1, 23–48.
2. Matkowsky, B.J.; Sivashinsky, G.I. Propagation of a pulsating reaction front in solid fuel combustion. *SIAM J Appl Math* 1978, 35, 465–478.
3. Brailovsky, I.; Sivashinsky, G.I. Chaotic dynamics in solid fuel combustion. *Phys D* 1993, 65, 191–198.
4. Munir, Z.A.; Anselmi-Tamburini, U. Self-propagating exothermic reactions: The synthesis of high-temperature materials by combustion. *Mater Sci Rep* 1989, 3, 277–365.
5. Frankel, M.; Roytburd, V.; Sivashinsky, G. A sequence of period doubling and chaotic pulsations in a free boundary problem modeling thermal instabilities. *SIAM J Appl Math* 1994, 54, 1101–1112.
6. Gross, L.K.; Yu, J. Weakly nonlinear and numerical analyses of dynamics in a solid combustion model. *SIAM J Appl Math* 2005, 65, 1708–1725.
7. Gross, L.K. Weakly nonlinear dynamics of interface propagation. *Stud Appl Math* 2002, 108, 323–350.
8. Yu, J.; Gross, L.K. The onset of linear instabilities in a solid combustion model. *Stud Appl Math* 2001, 107, 81–101.
9. Toth, Z.; Kalnay, E. Ensemble forecasting at NMC: The generation of perturbations. *Bull Am Meteorol Soc* 1993, 74, 2317–2330.
10. Danforth, C.M.; Kalnay, E.; Miyoshi, T. Estimating and correcting global weather model error. *Mon Weather Rev* 2007, 135, 281–299.